Wafer-scale photonic and plasmonic crystal sensors

M.C. George[*], J.-N. Liu[**], A. Farhang[*], B. Williamson[*], M. Black[*], T. Wangensteen[*], J. Fraser[*], R. Petrova[*] and B.T. Cunningham[**]

[*]Moxtek, 452 West 1260 North, Orem, UT, 84107, USA, mgeorge@moxtek.com
[**]University of Illinois, Urbana, IL, USA, bcunning@illinois.edu

ABSTRACT

Recent results in 200 mm diameter wafer-scale fabrication, metrology, and optical modeling of various photonic and plasmonic crystal sensors are presented, including 1-D photonic crystals based on leaky-waveguide mode resonance, as well as 1-D and 2-D metallic arrays based on surface plasmon resonance (SPR), with potential applications in label free sensing, surface-enhanced Raman spectroscopy (SERS), and surface-enhanced fluorescence spectroscopy (SEFS). Results include label-free photonic crystal and SPR sensing of bulk refractive index changes and modeling of surface binding sensitivity. In addition, SERS results are presented for 2D SPR arrays. Challenges in the commercialization of photonic and plasmonic crystal sensors are also reviewed.

Keywords: extraordinary optical transmission, SPR sensor, microarray, photonic crystal, label-free sensor

1 INTRODUCTION

Moxtek has leveraged existing capabilities in 200 mm diameter wafer-scale patterning of sub-wavelength wire grid polarizers into the fabrication of 1-D and 2-D periodic photonic and plasmonic crystal sensors, with potential applications in label free sensing, SERS, and surface-enhanced fluorescence spectroscopy (SEFS). Potential markets include micro-arrays for medical diagnostics, forensic testing, environmental monitoring, and food safety. Both fluorescence- and Raman-based spectroscopies serve as effective means of identifying and detecting molecules of interest in the bulk. However, for surface studies these methods typically offer relatively low signal-to-noise ratio (SNR) when specific enhancement approaches are not utilized. The use micro- and nano-structured metallic and dielectric arrays in the form of plasmonic and photonic crystals are two such enhancement approaches that can provide highly focused optical fields, thereby boosting the SNR by orders of magnitude and providing for enhanced fluorescence and Raman sensing capability at surfaces.

In this work, various types of nanostructures were fabricated, including 2-D metallic nano-hole arrays and 1-D grating-based photonic crystals for both fluorescence and label-free sensing applications, as well as 2-D nano-dome arrays for SERS. Figure 1 presents SEM images of 1-D photonic crystal and 2-D SPR sensor designs. The 1-D grating designs were composed of a TiO_2 slab waveguide layer despoited on top of a SiO_2 grating either etched directly into fused silica or etched into a sputter-deposited SiO_2 film on Silicon. The 2-D SPR gratings include tapered aluminum nano-hole arrays (NHA's) and gold-coated SiO_2 nano-dome arrays on glass substrates. The NHA was designed for both bulk refractive index (RI) sensing at 632.8 and 650 nm wavelengths and also as a label-free surface binding sensor at 532 nm. The SPR nano-dome arrays were designed to concentrate the incident electric field into "hot spots" that reside in the 5-15 nm gaps between nano-domes for SERS applications [1]-[2].

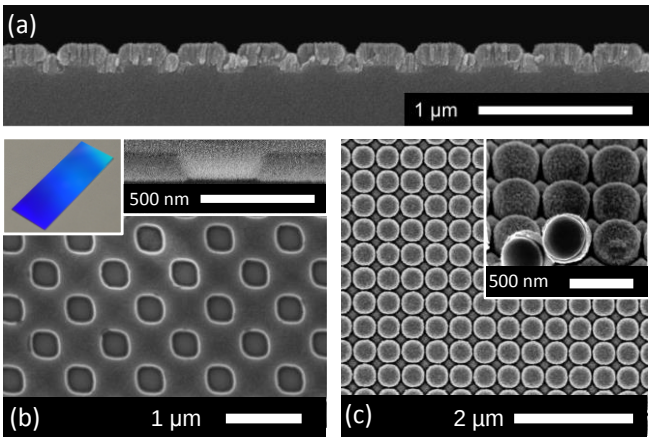

Figure 1: SEM analysis results for (a) 1-D photonic crystal sensor composed of TiO_2 layer on SiO_2 grating (in cross-section), (b) plan view tapered aluminum nano-hole array slide with photographic and cross-section insets, and (c) plan view gold-coated SiO_2 nano-dome arrays for SPR-enhanced SERS with perspective view inset.

2 METHODOLOGY

1-D and 2-D periodic nanostructures were fabricated on glass, fused silica, and silicon wafers using optical lithography and semiconductor processing techniques. Metrology included focused ion beam milling and SEM imaging, as well as normal incidence transmittance measurements in air and after immersion in water. Wafer-scale transmittance and reflectance mappping was performed at fixed angles in air for various polarization directions. Variable angle transmittance and reflectance measurements in air were also taken for certain samples. Where possible, surface binding was tracked using a

NanoSPR8 system with 637 nm laser diode. Fluorescence and Raman enhancement were evaluated for the 1-D gratings using a line-scan microscope system [3]. The 2-D nano-dome array SERS response was evaluated using a Renishaw inVia Raman microscope with 633 nm excitation. Optical modeling was performed using a commercial Finite Difference Time Domain (FDTD) package (Lumerical FDTD Solutions) and compared to experimental results. Rigorous Coupled Wave Analysis was also performed in certain cases (G-Solver and R-Soft) to speed analysis.

3 OPTICAL MODELING AND METROLOGY RESULTS

The NHA structures exhibit a plasmonic localization, allowing very strong enhancement of the illuminating light source, which is not only useful for surface enhanced fluorescence/Raman spectroscopy (SEFS and SERS), but also for surface plasmon resonance (SPR) sensing. Moxtek fabrication technology allows for easy variation of the structural dimensions such as pitch, hole size, and hole shape. This not only allows for a very large spectral tuning of the Bloch mode (grating-coupled) SPP resonances, as depicted in Figure 2(a), but also tuning of the strength and spatial distribution of the optical enhancement to suit a particular application and measurement configuration [4]. The ability of a NHA to optically sense variations in bulk refractive index via a change in the SPR wavelength is depicted in Figure 2(b), which presents experimental measurement results for a 0-40% glucose series using a 550 nm pitch Al NHA. The vertical dashed lines correspond to the design wavelength for an intensity based sensor, although these samples had tapered sidewalls for optimization of fluorescence enhancement [5]. The optical focusing and light enhancement mechanism behind SPR sensing is also responsible for the enhanced fluorescence and Raman Signals in SEFS and SERS. FDTD modeling of a protein binding in a 665 nm pitch Al NHA underwater is presented in Figure 2(c)-(d). In this case the protein was assumed to only cover the bottom 4 nm of the Al hole adjacent to the glass substrate. The refractive index was varied from the bulk value (1.33) to 1.475 in this region to simulate protein binding at the base of the hole. The shift in resonance depicted in Figure 2(c) is subtle and is best visualized in Figure 2(d) as the ratio of the transmittance spectra, which predicts almost a 5% relative drop in transmittance at 532 nm upon protein binding. While this intensity change should be reasonable enough to detect, experimental validation was not pursued as further design optimization has since improved this figure of merit considerably.

The optical structure depicted in Figure 1(a) is a type of grating-coupled leaky 1-D photonic crystal slab waveguide, also called a guided mode resonance filter [6]-[7], which gives a narrowband reflectance peak that is angle sensitive,

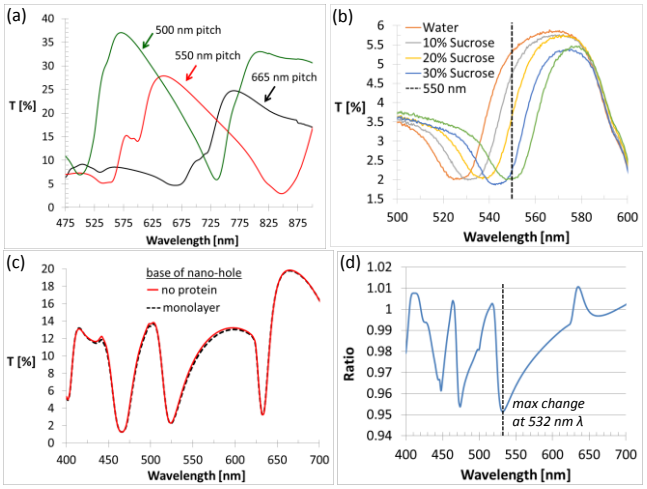

Figure 2: (a) Transmittance spectra for Al NHA's of varying pitch (500, 550, 665nm) demonstrating size tunability of spectral response. (b) Experimental transmittance results for varying glucose concentration (0-40 % aq.) in a 550 nm pitch Al NHA showing bulk refractive index sensitivity. (c)-(d) FDTD modeling for 665 nm pitch aluminum NHA in water before and after protein adsorption depicting (c) transmittance curves and (d) transmittance ratio.

especially when the plane of incidence is parallel to the grating vector. The resonanace is less angle sensitive when the plane of incidence is perpendicular to the grating vector (i.e. parallel to the grating lines)[8]. Figure 3(a) depicts experimental variable angle of incidence (AOI) s-polarized reflectance results (from 7.5° - 65°) for such a case, while the wafer maps presented in parts 3(b)-(c) depict 7.5° AOI s-polarized reflectance peak height and peak wavelength uniformity over a 200 mm diameter wafer. Manufacturing process variability can result in slight changes in SiO_2 grating etch depth, duty cycle, and TiO_2 layer thickness, which can result in slight changes in resonance wavelength, peak height, and FWHM. Resonator quality factor is thus dependent on these manufacturing conditions. Because of

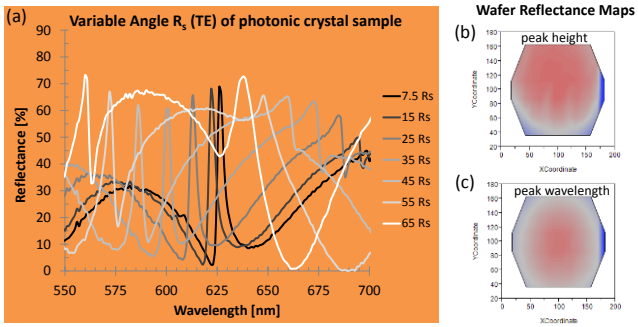

Figure 3: (a) Experimental variable angle of incidence (AOI) reflectance results for s-polarized light in a narrow band photonic crystal resonance sensor. (b)-(c) Wafer maps for 7.5° AOI reflectance showing (b) peak height and (c) peak wavelength uniformity. Red color corresponds to larger Reflectance or longer λ.

the angle sensitivity of these guided mode resonance filters, proper beam collimation is critical when characterizing the spectral reflectance of these structures or else the quality factor will be under-estimated. An example of this can be seen in figure 4, where 1-D photonic crystal samples on fused silica (4a) and on silicon (4b) were characterized in reflectance on two different tools. Both tools used a known reflectance reference sample to generate normalized reflectance curves, but the tool represented by the dashed lines had poorer beam collimation and insufficient spectrometer resolution to resolve the narrow peaks, especially in the case of the samples on silicon, which had narrow resonanace linewidths. The slight blue shift is due to a 2.5° difference in AOI in the two instruments.

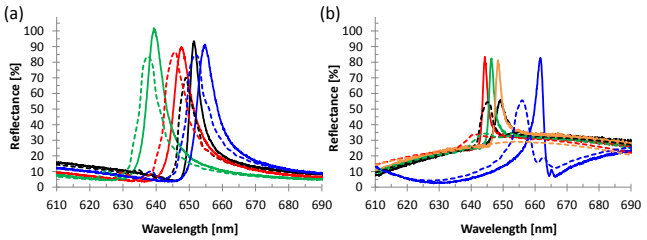

Figure 4: Differences in 1-D photonic crystal slab waveguide reflectance metrology. (a) Initial wafer-to-wafer variation in 1-D photonic crystals fabricated on fused silica for SERS applications (b) Initial intra-wafer variation (center to extreme edge positions) in 1-D photonic crystal fabricated on silicon wafer for SEFS applications. The dashed measurements were taken at the wafer level at 7.5° AOI with poorer beam collimation and coarser spectrometer resolution. The solid lines were taken at the chip level with improved collimation, better alignment, and finer spectrometer resolution.

The 2-D nano-dome array structures depicted in Figure 1(c) were designed for SERS applications and are sensitive to the nano-gap between adjacent domes. One batch of wafers had a rougher gold coating, which appeared darker in color, and those samples showed flatter reflectance spectra. The other batch of wafer had a more golden color and the films appeared much smoother under SEM imaging. Figure 5 depicts metrology and application results for some of these samples. Figure 5(a) depicts the reflectance behavior and reveals that only the smooth films show the expected SPR resonance feature. Part 5(b) depicts the SERS spectra for a rougher gold-coated nano-dome array sample in blue and a smoother nano-dome array sample in red. The smoother nano-dome array structure with the better optical properties has the better resolved Raman vibrational mode peaks.

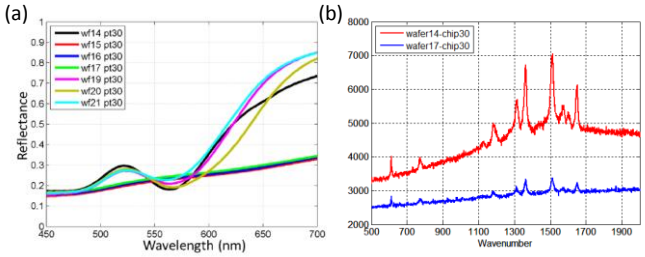

Figure 5: (a) Reflectance spectra for various SPR nano-dome array samples. (b) Corresponding SERS spectra for two of the samples after coating with a dye.

4 CONCLUSIONS

Moxtek has leveraged existing capabilities in wafer-scale patterning of sub-wavelength wire grid polarizers into the fabrication of 1-D and 2-D periodic photonic and plasmonic crystal sensors, with potential applications in label free sensing, SERS, and SEFS. Resonance wavelengths can be tuned by varying the pitch or feature size. An intensity-based NHA SPR sensor showed good bulk refractive index sensitivity in the red spectral region and decent surface sensitivity at 532 nm. 1-D photonic crystal devices showed the expected angular response, which made accurate metrology more challenging. Narrow band resonance peaks were resolved using an improved metrology setup with better beam collimation and finer spectrometer resolution. Wafer mapping of optical properties revealed that processing variation was impacting uniformity. 2D nano-dome arrays showed enhanced Raman signal when the gold film quality was good.

REFERENCES

[1] H.-Y. Wu, B.T. Cunningham, Nanoscale, 6, 5162, 2014.

[2] H.-Y. Wu, C.J. Choi, B.T. Cunningham, Nanoscale, 8, 2769, 2012.

[3] S. George, et al**.,** Lab Chip, 13, 4053, 2013.

[4] M.C. George, et al., Proc. SPIE, 9163, 91633B-1, 2014.

[5] M. Diwekar, et al., J. of Nanophotonics, 4, 043504, 2010.

[6] L. Mashev and E. Popov, Opt. Commun. 55, 377, 1985.

[7] B.T. Cunningham, P. Li, L. Bo, , J. Pepper, The 15th IEEE International Conference on MEMS, 2002, 64-68, 2002.

[8] A.K. Kodali, et al., Anal. Chem. 82, 5697, 2010.